Reducing seed dependent variability of non-uniformly sampled multidimensional NMR data

Mehdi Mobli

Centre for Advanced Imaging, The University of Queensland, St. Lucia, QLD 4072, Australia

Abstract

The application of NMR spectroscopy to study the structure, dynamics and function of macromolecules requires the acquisition of several multidimensional spectra. The one-dimensional NMR time-response from the spectrometer is extended to additional dimensions by introducing incremented delays in the experiment that cause oscillation of the signal along "indirect" dimensions. For a given dimension the delay is incremented at twice the rate of the maximum frequency (Nyquist rate). To achieve high-resolution requires acquisition of long data records sampled at the Nyquist rate. This is typically a prohibitive step due to time constraints, resulting in sub-optimal data records to the detriment of subsequent analyses. The multidimensional NMR spectrum itself is typically sparse, and it has been shown that in such cases it is possible to use non-Fourier methods to reconstruct a high-resolution multidimensional spectrum from a random subset of non-uniformly sampled (NUS) data. For a given acquisition time, NUS has the potential to improve the sensitivity and resolution of a multidimensional spectrum, compared to traditional uniform sampling. The improvements in sensitivity and/or resolution achieved by NUS are heavily dependent on the distribution of points in the random subset acquired. Typically, random points are selected from a probability density function (PDF) weighted according to the NMR signal envelope. In extreme cases as little as 1% of the data is subsampled. The heavy under-sampling can result in poor reproducibility, i.e. when two experiments are carried out where the same number of random samples is selected from the same PDF but using different random seeds. Here, a jittered sampling approach is introduced that is shown to improve reproducibility of multidimensional spectra generated from NUS data, compared to commonly applied NUS methods. It is shown that this is achieved due to the low variability of the inherent sensitivity of the random subset chosen from a given PDF. Finally, it is demonstrated that metrics used to find optimal NUS distributions are heavily dependent on the inherent sensitivity of the random subset, and such optimisation is therefore less critical when using the proposed sampling scheme.

Keywords: Non-uniform sampling, multidimensional NMR, jittered sampling, Poisson-gap sampling, sine-weighted sampling, exponentially weighted sampling

Non-standard abbreviations:
Jittered Sampling (JS)
Poisson-gap Sampling (PS)
Random Sampling (RS)
Exponentially-weighted Jittered Sampling (EJS)
Exponentially-weighted Random Sampling (ERS),
Sine- and Exponentially-weighted Sampling (SEJS)
Probablity Density Function (PDF)
Peak-to-Sidelobe Ratio (PSR)
Point-Spread-Function (PSF)
NonUniform Sampling (NUS)

Author for correspondence:
Mehdi Mobli, email: m.mobli@uq.edu.au, tel: +61 7 334 60352

1. Introduction

Multidimensional NMR experiments are a prerequisite in the study of complex biomolecules. Introduction of isotope labelling and the design of triple resonance experiments have been critical in establishing the biomolecular NMR field [1]. Recent improvements in spectrometer hardware, including ultra-high field and cryogenically cooled probes have significantly improved the sensitivity of multidimensional NMR experiments, making NMR a routine method for structural studies of biomolecules.

As the application of NMR to study biomolecules increases so does the pressure on improving the throughput of multidimensional experiments. The 1D NMR signal, which is acquired in real time, is extended to multiple dimensions by iteratively incrementing delays in the multidimensional experiments to generate additional "indirect" dimensions. The length of the data record along each indirect dimension (evolution time) dictates the resolution attainable in that dimension. However, accurate processing of the time domain data into a frequency spectrum using the Fourier transform requires sampling of the time domain at uniform intervals at twice the rate of the highest frequency signal (Nyquist rate). Thus, in order to obtain high-resolution spectra it is necessary to sample the time domain at uniform intervals and for a long time period. These constraints result in very long acquisition times to generate high-resolution multidimensional NMR spectra. Typically up to ten 3D experiments are required to solve the structure of a protein, each requiring days of spectrometer time to achieve the necessary resolution.

To increase the throughput of NMR experiments several methods have been introduced that aim to reduce the acquisition time by relaxing some of the above-mentioned sampling requirements [2]. Perhaps the most general of these is by non-uniform sampling (NUS) of the time domain data. This can be considered as sub-sampling the complete time domain grid as dictated by the Nyquist condition (Nyquist grid). Omission of sample points results in a compressed dataset and it has been shown that if the information content (number of signals) is sparse it is possible to faithfully reconstruct the frequency domain spectrum from such a sparse dataset using various non-Fourier processing methods, including maximum entropy reconstruction [3], CLEAN [4], multidimensional deconvolution [5], multidimensional FT [6], iterative soft thresholding [7] and compressed sensing [8, 9].

NUS is primarily used to reduce the required experiment time, such that high-resolution spectra can be obtained from an NUS subset [10]. Alternatively, NUS can be used to boost the sensitivity of NMR experiments by acquiring more repetitions of the experiment whilst sampling fewer time points. Under particular conditions it is possible to boost both sensitivity and resolution by use of NUS [11-13].

The spectra generated from NUS data are to an extent dependent on the processing method used, but are also to a large extent dependent on the distribution of the sampled points. For example, it has been shown that the characteristic ridge artifacts associated with back-projection reconstruction (BPR) are due to the distribution of the samples in the time domain, and are present in spectra generated by other reconstruction methods [14].

The significant impact of the sampling distribution on the reconstructed spectrum has led to various approaches aimed at optimising the distribution of NUS data. Certain trends have become apparent, including results showing that periodicity in the distribution leads to prominent artifacts, which can be effectively reduced by introducing disorder [15]. There is, however, no consensus on an optimal sampling method. The earliest and perhaps most robust approach to NUS is random sampling from an exponential probability density function (PDF) that mimics the natural decay of the NMR signal [16]. This is analogous to a window function with a decay rate corresponding to the linewidth of the NMR signal (matched filter). In analogy to windowing of NMR signals, applying decay rates that are slower than that of the measured signal result in sharper signals (narrow linewidth) but noisier spectra, whilst applying decay rates faster than those of the measured signal produce higher sensitivity spectra with lower resolution (broad linewidth) [17]. The choice of decay rate is, therefore, in much the same way as with window functions, dependent on the experiment. More recent studies have explored the potential for improving sensitivity by non-uniform sampling

using different PDFs and formal relationships between these distributions and their intrinsic sensitivity have been derived [18].

The above procedure provides an avenue for comparing the relative sensitivity of different PDFs, however, it does not provide any information on how variable the results are where different random subsets are chosen from the same PDF. For example, where the Nyquist grid is defined, and a defined number of samples are drawn from a given PDF, there remains a random seed dependent variation in the distribution of the samples drawn, which is only dependent on the random seed used. This variability becomes particularly pronounced where the data is heavily under-sampled and raises reproducibility issues when NUS is applied to multidimensional NMR experiments. It is for example possible that if an NUS experiment is reported in the literature together with all the relevant parameters used to generate the random subset, the same results may not be replicated independently without knowledge of the actual subset drawn (commonly referred to as the sampling schedule).

It is generally accepted that this random seed dependent variability can be very significant, to the point where it has become a common approach to optimise NUS schedules using random search (e.g. Monte Carlo) approaches. The optimisation is carried out by defining a given quality measure of the sampling distribution (or in a transform space of that function), which is subsequently used to rank a large number of generated schedules [19]. The quality measure is commonly evaluated based on the point-spread-function (PSF) of the sampling function. The sampling function is a binary function where ones are used to denote sampled points and zeroes represent omitted data points in a predefined Nyquist grid. The Fourier transform of the sampling function then results in the PSF. The PSF contains a signal at 0 Hz frequency and sampling noise outside of this frequency. The artifacts due to NUS in experimental data originate from the convolution of the PSF with the measured NMR signals. Thus, the intensity and distribution of the sampling noise serves as a useful tool in evaluating different sampling functions. To date there is no universal measure of the quality of a PSF and common metrics used, include the peak to side-lobe ratio (the ratio between central component of the PSF and the most intense artifacts) and the level of sampling noise in some region of the PSF [10]. The lack of a consensus quality metric will inevitably lead to disagreement about the appropriateness of any given metric used.

Several pseudo-random sampling methods including jittered, Poisson disc and Poisson gap sampling have been suggested that also reduce the random seed dependent variability of the sampling noise [19-22]. The jittered sampling and Poisson based (gap and disc) sampling approaches are closely related. The Poisson disc method imposes the highest degree of order on the distribution of sampling points. The method can be described as sampling a particular point and then imposing a region about this point that may not contain another sample, successive samples are added in "allowed" regions until the required number of points have been selected. In the extreme case this can become a problem, for example, when exactly half the points in a discrete 1D series (spaced uniformly) are to be retained randomly, the method would necessarily retain every other point (either with the first point sampled or not), resulting in perfect aliasing.

To overcome this limitation, the Poisson gap method ensures sampling points follow a Poisson distribution [$f(k;\lambda) = (\lambda^k e^{-\lambda})/k!$], i.e. that the probability of finding a sample point in a given region adheres to a Poisson distribution. It is therefore possible to sample two adjacent points, albeit with a low probability [21]. This sampling method, as introduced to NMR by Hyberts *et al.*, is further weighted to produce a sine-weighted distribution (0 to $\sin(\pi)$ over the desired Nyquist grid). The use of the sine weighting penalises values having high values of $\sin(x)$, thus it can be considered to impose a PDF having a $\pi/2$ shifted sine function. This distribution was motivated by a desire to avoid gaps at the beginning and end of the sampling schedules, which were anecdotally considered to be particularly bad when processing NUS data using forward maximum entropy (FM). The weighting was then modified to span 0-$\sin(\pi/2)$ for exponentially decaying NMR signals resulting in a distribution very similar to an exponentially weighted distribution (albeit with a Poisson distribution). In 2D, the Poisson gap method can be extended by employing the 1D Poisson gap algorithm along individual rows and columns, in a "woven" manner [23]. However, as each

column/row is treated individually, there is no constraint to adhere to a Poisson distribution between rows, thus the distribution in 2D does not necessary result in sampling points drawn from a Poisson distribution.

The implementation of jittered sampling in NMR by Kazimierczuk *et al.* divides the time domain into square segments [20]. The number of segments, referred to as cells, determines the number of samples, and the size of each cell in turn depends loosely on the PDF. The method is an off-grid method and samples are allowed to occur at an arbitrary position inside the defined cell. It is unclear how the PDFs are related to the cell sizes and how this would behave for complex multidimensional PDFs with different weighting along different dimensions.

All of the above methods have the desirable property that they reduce the seed dependent variability of the sampling schedules, be it with some caveats. The Poisson based methods reduce the inherent disorder in the sampling, ultimately leading to aliasing in the extreme case. Whilst the Poisson gap sampling method overcomes this to an extent in the 1D case, it is unclear how the current implementation achieves a Poisson distribution in the multidimensional case. The Monte-Carlo method is an appealing approach but in the absence of definitive quality measures it is difficult to optimise.

Here a general algorithm is introduced based on jittered sampling, which is appropriate for on-grid sampling and applicable to arbitrary PDFs along arbitrary number of dimensions. The algorithm does not segment the PDF into regions using defined geometrical shapes but instead defines regions based on the underlying PDF. Notably, this treatment ensures that all NUS distributions based on the same PDF have nearly identical inherent sensitivity. The performance of the algorithm is compared in the one-dimensional case to random exponential sampling as well as Poisson gap sampling through analysis of the PSFs generated by the different approaches.

Examples of jittered sampling in experiments with two indirect dimensions are demonstrated (3D experiments). The approach provides a robust general method for non-uniform sampling with minimal seed dependence whilst introducing minimal order in the sampling. Using experimental data, it is shown that the proposed jittered sampling method improves the reproducibility of NMR experiments where NUS is applied.

2. Theory & Methods

Random samples from a probability distribution

The sampling schedules are generated based on the single pass method described previously [24]. First, a Nyquist grid is defined, consisting of L dimensions each having T_k points along the k^{th} dimension. The total size of the grid (N) is defined by the product of the number of points along each dimension:

$$N = \prod_{k=1}^{L} T_k \qquad (1)$$

The distance between adjacent points in each dimension is defined by the dwell time D_k (equivalent to $1/sw_k$, where sw_k is the spectral window/width along the k^{th} dimension). The probability ($p(i)$) associated with each point (i) on the Nyquist grid is calculated based on the desired PDF, i.e. exponential decay for regular NMR acquisition:

$$p(i) = \prod_{k=1}^{L} e^{-i\pi lw_k / sw_k} \qquad (2)$$

where lw_k and sw_k are the linewidth and spectral window in the k^{th} dimension, respectively, and the equation may be further altered to include, for example, J modulation. The single pass method described previously then calculates a rank for each point $r(i)$ according to:

$$r(i) = x(i)^{1/p(i)} \quad (3)$$

where $x(i)$ is a random number between 0 and 1. The rank $r(i)$ is then sorted in descending order. The number of points subsampled from N is defined as m, where $m \leq N$. In the single pass approach the top m points would represent random points from the defined exponential distribution. When samples are selected from an exponentially decaying PDF according to the ranks of Eq. 3, it is referred to here as exponential random sampling (ERS).

Jittered sampling from a probability distribution

The jittered sampling approach implemented here, is suitable for any arbitrary PDF for arbitrary number of dimensions. First $p(i)$ are normalised within the bounds of the space such that the sum of all weights is equal to 1 producing normalised weights:

$$p'(i) = \frac{p(i)}{\sum_{i=1}^{N} p_i} \quad (4)$$

The probability space is then divided into m parts, where $1/m$ defines the total probability of each region. Within each region a point is selected either randomly or according to its rank as defined by Eq. 3. In practice the algorithm is implemented as follows:

The Nyquist grid as defined above by the elements of $p'(i)$, is segmented into jittered regions. The jittered regions are each a subset of the Nyquist grid. Each jittered region is defined by selecting points form the Nyquist grid according to the below algorithm, where ***Y*** is a temporary array that is filled with elements (coordinates) until a region is defined.

1. Pick the point y_j with the highest probability as defined by p' and add this to ***Y***.
- *a*. Identify the neighbours of y_j (coordinate preceding or following y_j along each dimension on the Nyquist grid)
- *b*. Pick the neighbour of y_j with the highest probability from p' and stores this as y_{j+1}.
  - *i*) If multiple points have the same (highest) probability then pick the one closest to the centroid of ***Y***
- *c*. Calculate the sum of probabilities of all elements of ***Y*** including the contribution of y_{j+1}.
  - *i*) If inclusion of (y_{j+1}) results in a total probability that is closer to $1/m$ then add y_{j+1} to ***Y***, increment j and repeat from *a* (i.e. find neighbours of added point).
  - *ii*) If *c.i*) is not true, then the elements of ***Y*** define a jittered region. Pick the point from ***Y*** with the highest rank (as defined in Eq. 3), store the coordinates of this point in the sampling schedule. Remove all elements of ***Y*** reset j to 1 and remove all points defined in this region from the Nyquist grid, so that these cannot be reselected in subsequent regions. If there are any points left on the Nyquist grid define a new region by returning to 1.

Algorithm. Steps involved in drawing jittered samples from a multidimensional, weighted probability distribution.

After each region is defined a residual remains which is the difference between the sum of the probability (as defined by p') of all points in that region and $1/m$. The residual is carried over and used to redefine the region sizes for the remaining iterations, this ensures that rounding errors are not propagated. Also note that *1.c.ii* uses the probability as defined in Eq. 3, this will ensure that the

probability distribution is also taken into account within each region. In the 1D case if a large proportion of the defined grid is sub-sampled, this can increase the probability of generating strong aliasing artifacts, thus in 1D, the samples are here simply taken as a random point in each region. In the software implementation of the algorithm, this is treated as a user defined parameter (which practically, involves modification of Eq. 3 to produce random ranks). Where jittered sampling is applied to an exponentially decaying probability distribution according to Eq. 2, it is referred to as "exponential jittered sampling" (EJS).

Extension of the above algorithm to multiple dimensions is straightforward although two slight modifications are made. To avoid cases where a small region is confined between already defined regions such that it does not have any further neighbours, the points in that region are merged with a neighbouring region; again the appropriate residual probability is used to redefine region sizes in subsequent iterations (same is true if a point is not assigned to a region). Finally, at step *b.i*. the point closest to the centroid of the region is only calculated where two neighbours have the same probability, this leads to narrow regions for any weighted PDF. To avoid this, a threshold probability difference (set by default to 1/N) between the evaluated points is defined, and points within this threshold are considered in step b.*i*. to be equal and the one closest to the centroid of the region is chosen.

Relative sensitivity & resolution of a sampling schedule

Comparison of different sampling schedules generated using different NUS methods, e.g. Poisson gap sampling *vs* random sampling, requires that these have comparable properties, in particular with respect to sensitivity and resolution. Various measures have been proposed for measuring the relative sensitivity of a sampling schedule. Rovnyak *et al.* have shown that where the probability function of NUS data can be defined precisely it is possible to derive an analytical solution to SNR enhancement for different weighting functions [25]. The decay function of Poisson gap sampling is complicated by the adjustable weighting parameter (w) that ensures Poisson distribution of the generated points without strictly requiring these to adhere to the specified weighting function [21]. It is therefore difficult to define the PDF of Poisson gap sampling hence also defining an exponential weighting scheme that would be equivalent to a particular Poisson gap sampling scheme.

Instead comparable schedules may be defined as having the same relative sensitivity as described previously [18]:

$$R(\boldsymbol{K}) = \frac{\sum_{i=1}^{N} k_i p_i}{\sum_{i=1}^{N} p_i} \qquad (5)$$

where $\boldsymbol{K}$ is the sampling function, k_i has the value 1 for sampled times and zero for times not sampled and p_i is as defined in Eq. 2. $R(\boldsymbol{K})$ is a good measure of sensitivity but it does not take into account the contribution from the experimental noise. For example, consider the case where a Nyquist grid is defined as having 100 points but where the first 10 points contain the entire probability density (points 11 to 100 have 0 probability of containing a signal). In this case it does not matter if one sub-samples the first 10 points or all 100 points, the value of $R(\boldsymbol{K})$ is 1 when using Eq. 5. In reality the latter case, where all 100 points are sampled, would also result in a higher noise contribution, which is not reflected in $R(K)$. To overcome this issue, $R(\boldsymbol{K})$ is here scaled by N/m, such that $R'(\boldsymbol{K}) = R(\boldsymbol{K})\times(N/\mathrm{m})$. Using the modified $R'(\boldsymbol{K})$ function it is now possible to distinguish the two cases above, such that if the first 10 out of 100 points are selected and these contain all of the probability, $R'(\boldsymbol{K})$ becomes 10. That is, a factor of 10 difference (in time savings) when only sampling the first 10 points compared to sampling all 100 points.

The $R'(\boldsymbol{K})$ measure does, however, not reflect the resolution enhancement achieved by the NUS scheme. A suitable measure of resolution enhancement should take into account the

distribution of the samples, in particular with respect to the proportion of samples at long evolution times. Here the average and median evolution times (A_{ev} and M_{ev} respectively) are proposed as useful metrics for measuring the resolution enhancement achieved by a sampling schedule. These parameters are further normalised by dividing them by the longest evolution time as defined by the Nyquist grid (T_k). This results in a value that will always be between 0 and 1, where values towards 0 reflect a sampling schedule with low resolution enhancement, whilst values close to 1 reflect those providing a high level of resolution enhancement, and a linear sampling scheme that samples all points until N will produce a value of 0.5.

Although the decay parameters (related to ^{lw_k}) of EJS and ERS can be adjusted to achieve the same relative sensitivity as measured by $R'(\boldsymbol{K})$, this cannot be achieved while maintaining similar resolution parameters (A_{ev} and M_{ev}). Here, we will compare different sampling strategies (e.g. ERS *vs* EJS) by adjusting the variable parameters (e.g. ^{lw_k}) until the same relative sensitivity, $R'(\boldsymbol{K})$, is achieved. A_{ev} and M_{ev} will be reported to reflect differences in the distribution of points between the different approaches.

Approximation of sine weighted Poisson-gap sampling

As previously described, the schedules generated using PS are sine weighted and thus have a stronger weighting at short and long evolution periods. Thus, although an EJS/ERS sampling schedule with the same relative sensitivity, $R'(\boldsymbol{K})$, as PS can be produced, it will not have a similar distribution as defined by A_{ev} and M_{ev}. Instead the distribution of PS can be emulated in EJS and ERS by introducing a shifted sine weighting, attenuating the PDF (Eq. 2) by scaling down the central region. The following function:

$$\alpha \sin^{\beta} \pi \left(\frac{1}{2} + \frac{i}{N}\right) + (1 - \alpha) \qquad (6)$$

when multiplied by Eq. 2 was found to yield sampling schedules with distributions in close agreement with those generated by the PS (see Fig. 1). The α parameter in the above equation is a real valued scaling, determining how much the central region of the probability distribution will be scaled down. The β parameter is an even integer and determines the width of the central region being scaled down. Where Eq. 6 is applied to EJS the sampling function is referred to as sine-weighted exponential jittered sampling (SEJS).

Where sine weighting is applied to multiple dimensions the product of Eq. 6 along each dimension results in a weighting that has the highest probability at the intersection of the extremes of each time axis (or corners of the multidimensional object). The purpose of the sine weighting is to increase the probability at the edges of the object not the corners. In the implementation used here this is achieved by evaluating Eq. 6 for all dimensions of the multidimensional object and only multiplying Eq. 2 by the highest value.

Sampling artifacts and the point-spread-function

The PSF serves as a useful tool to predict the distribution and intensity of the artifacts related to NUS. A common measure proposed for quantitating the noise content of a PSF is the peak-to-sidelobe ratio (PSR). However, this does not provide a good measure of the total noise present, instead it provides a measure of the highest amplitude artifact to be expected from each signal in the spectrum. To provide a measure for the total noise associated with the PSF, the average of the magnitude spectrum was calculated (which can also be considered to be the average of the Euclidian norm of the complex numbers or the average l_1 norm of the magnitude spectrum):

$$\bar{M}_{PSF} = \frac{\sum_{i=1}^{N} \sqrt{Re_i^2 + Im_i^2}}{N} \quad (7)$$

where *Re* and *Im* are the real and imaginary components of the PSF. We also note that the 0 Hz frequency signal should be excluded. The width of this signal is dependent on the distribution of the data points and is loosely related to the average and median evolution times (as defined above). The width was evaluated manually to ensure that only the "noise" was included in sidelobe part of the PSR and the $\bar{M}_{PSF}$ parameters. The standard deviation σ_{PSF} from the $\bar{M}_{PSF}$ was also calculated. The moving average as defined recently [26] was also calculated, however, this produced trends in close agreement with the $\bar{M}_{PSF}$ parameter and was not considered further.

Methods

The jittered sampling algorithm as well as sine weighting of the PDF were incorporated into a computer program called sched3d (version 5), written in C [24]. All synthetic data were generated using the *Rowland NMR toolkit version 4* (http://rnmrtk.uchc.edu/rnmrtk/RNMRTK.html). Spectra were plotted using the functions within the *Rowland NMR toolkit*. The heat map representation of the jittered regions was generated using *Gnuplot* (http://www.gnuplot.info). The spectrometer implementation (on a Bruker spectrometer running *Topspin 3.0*,) of this code was done using an AU program called *nus_mm.be*. *Sched3d5* and *nus_mm.be* are available from the author upon request. The script generates a set of prompts for user input related to the variations of jittered sampling as described above (e.g. linewidth parameters and sine-weighting), whilst reading the appropriate parameters from the experiment (Nyquist grid size, spectral windows etc.). These parameters are compiled and used to generate a sampling schedule that is stored appropriately for execution of the experiment. The experimental data was generated as previously described [14] from a commercially obtained (AVR) sample of uniformly $^{15}N/^{13}C$ labelled ubiquitin at a concentration of ~1mM and a pH of 6.5 at nominal ^{1}H frequency of 600 MHz on a Varian spectrometer equipped with a cryogenically cooled probe. This data was processed using the maximum entropy reconstruction method as implemented in the *Rowland NMR toolkit*.

3. Results

1D schedules

The 1D Poisson gap sampling code as published previously [21] was used to generate a series of Poisson distributed sampling (PS) schedules, where 128 points were subsampled from a total of 512 points. The spectral parameters used were a *sw* of 6000 Hz and at a spectrometer frequency of 600 MHz (resulting a 10 ppm window). The average of *R'(**K**)*, as well as A_{ev} and M_{ev} were monitored over 1000 generated schedules. This resulted in average values of *R'(**K**)* = 1.23 (±0.01), A_{ev} = 0.34 (±0.01) and M_{ev} = 0.25 (±0.02). Two other sets of 1000 sampling schedules were generated, one using ERS and another using EJS (as described above). The *lw* parameters for ERS and EJS were adjusted to produced average *R'(**K**)* parameter matching those of PS (see Table 1). The *lw* parameters were found to be 9.5 and 8.2 Hz for ERS and EJS respectively. Two further sets of 1000 schedules were generated using SEJS, both adjusted to have average *R'(**K**)* parameters matching those of PS. The first, "SEJS1", was chosen to approximate the sample distribution of PS as described by A_{ev} and M_{ev} and the second, "SEJS2", further exaggerates the sine-weighting at early and late evolution times. SEJS1 was generated using α and *β* parameters of 0.6 and 8 (Eq. 6) together with a *lw* parameter of 5.5 Hz (Eq. 2). SEJS2 was generated using *α* and *β* parameters of 0.7 and 12 respectively, and an *lw* parameter of 4.9 Hz. The various metrics for these schedules are also summarised in Table 1.

Fig. 1 shows plots of a representative sampling schedule generated with the above parameters for ERS (blue diamonds), PS (green triangles), EJS (black squares), SEJS1 (orange

pluses) and SEJS2 (red dots). As can be seen that the EJS method mimics the distribution of ERS whilst SEJS1 follows that of PS well, finally we can see that SEJS2 further enhances the sine weighting seen in PS.

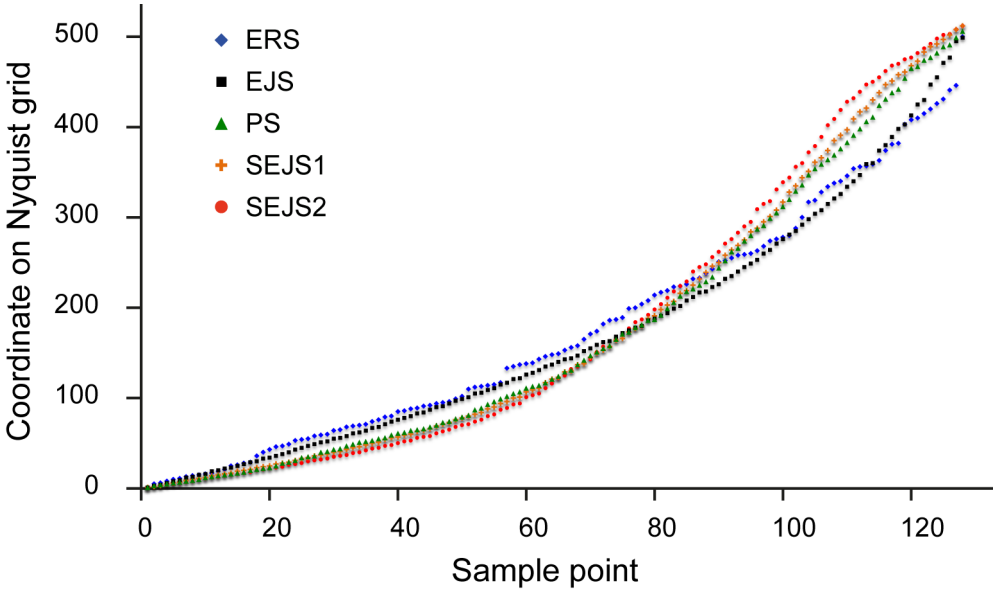

Figure 1 *The sampling schedule is a vector containing the coordinates to be sampled along a predefined Nyquist grid. The sampling schedule for different NUS schemes are plotted, with the index of the point being sampled on the y-axis and the index of the sampling schedule on the x-axis. Exponentially weighted random sampling (ERS) is represented by blue diamonds, exponentially weighted jittered sampling (EJS) by black squares, sine and exponentially weighted jittered sampling which approximates Poisson gap distribution (SEJS1) by orange pluses, sine and exponentially weighted jittered sampling which exaggerates the sine weighting of Poisson gap distribution (SEJS2) by red dots and Poisson-gap sampling (PS) by green triangles.*

Table 1 *The average and standard deviation of sampling schedule related parameters. 1000 sampling schedules were generated using different random seeds for five different NUS approaches. ERS: random samples from an exponentially decaying probability distribution. EJS: jittered random samples from an exponentially decaying probability distribution. PS: Poisson gap sampling with shifted sine weighting. SEJS1: jittered random samples from an exponentially decaying probability distribution augmented with a shifted sine weighting. SEJS2: same as SEJS1 but with different decay and sine weighting.*

	ERS	EJS	PS	SEJS1	SEJS2
R'(K)	1.23	1.23	1.23	1.23	1.23
St. dev.	0.03	0.00	0.01	0.00	0.00
A_{ev}	0.33	0.33	0.34	0.35	0.35
St. dev.	0.02	0.00	0.01	0.00	0.00
M_{ev}	0.27	0.27	0.25	0.23	0.22
St. dev.	0.03	0.00	0.02	0.00	0.00

The data in Table 1 shows that although the mean of *R'(**K**)* is kept the same for all NUS approaches, ERS has a much higher standard deviation of *R'(**K**)* values about the mean compared to EJS. This reflects the random seed dependence of ERS and suggests that it is significantly reduced in EJS. This large variation can lead to significant differences in the spectra generated from the extremes of the distribution. To exemplify this the sampling schedule resulting in the highest

and lowest value of *R'(**K**)* for ERS and EJS were compared (Fig. 2). The results show that larger seed dependent variation of *R'(**K**)* when using ERS leads to noticeable difference in the PSF. In contrast the low variation of *R'(**K**)* when using EJS, results in little seed dependent change of the PSF. When these differences are quantified a correlation between the sampling schedule realted parameter *R'(**K**)* and the PSF related parameters of resolution (linewidth) and sensitivity ($\overline{M}_{PSF}$) can be seen.

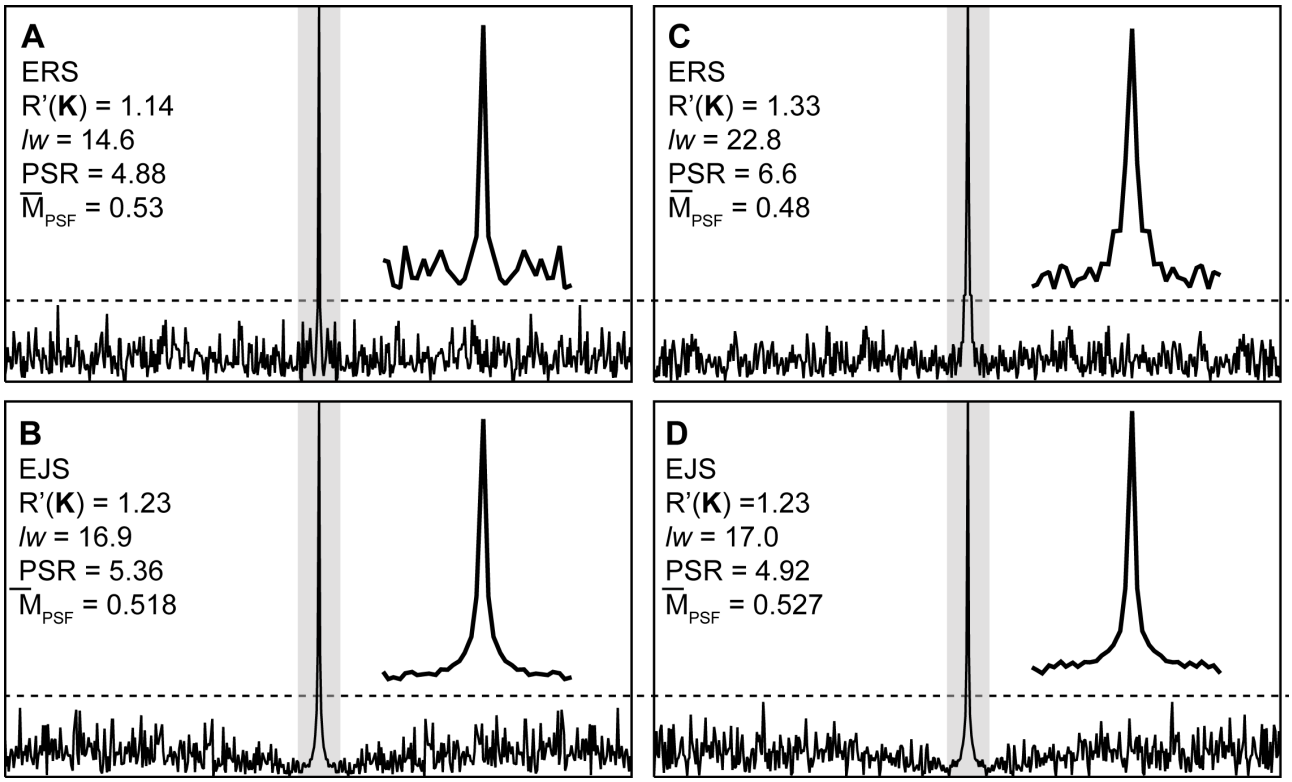

Figure 2 *Random seed dependence of relative sensitivity, as measured by R'(**K**), for ERS (A/C) and EJS (B/D) sampling. 1000 sampling schedules were generated with identical parameters but different random seeds. The PSFs corresponding to the sampling schedules with the lowest (A/B) and highest (C/D) R'(**K**) are shown. The sampling strategy as well as R'(**K**), the measured linewidth (lw) of the central component, the peak-to-sidelobe ratio (PSR) and the average of the magnitude spectrum ($\overline{M}_{PSF}$) is reported in all cases. The inset shows an expansion of the central component (shaded). The dashed line is at the same relative position in all windows and marks the highest amplitude artifacts across all four PSFs.*

The seed dependent variation of *R'(**K**)*, A_{ev} and M_{ev} is further shown for the first 100 schedules of the 1000 schedules generated (Fig. 3). In all cases the jittered sampling methods show very little seed dependence, whilst PS shows slightly less variation then ERS. Compared to ERS and EJS the sine-weighted sampling methods (PS, SEJS1 and SEJS2) consistently show higher median evolution times and lower average evolution times, consistent with these having a distributions skewed to the right. There is also a very clear correlation between the relative sensitivity, *R'(**K**)*, and the average evolution time A_{ev} for ERS and PS, which is not present for the jittered sampling methods (due to the small seed dependence of these parameters). The correlation between *R'(**K**)* and A_{ev} suggests that the higher sensitivity of certain PS/ERS schedules is related to increased sampling at early time points and is therefore also likely to result in increased linewidths, hence lower resolution.

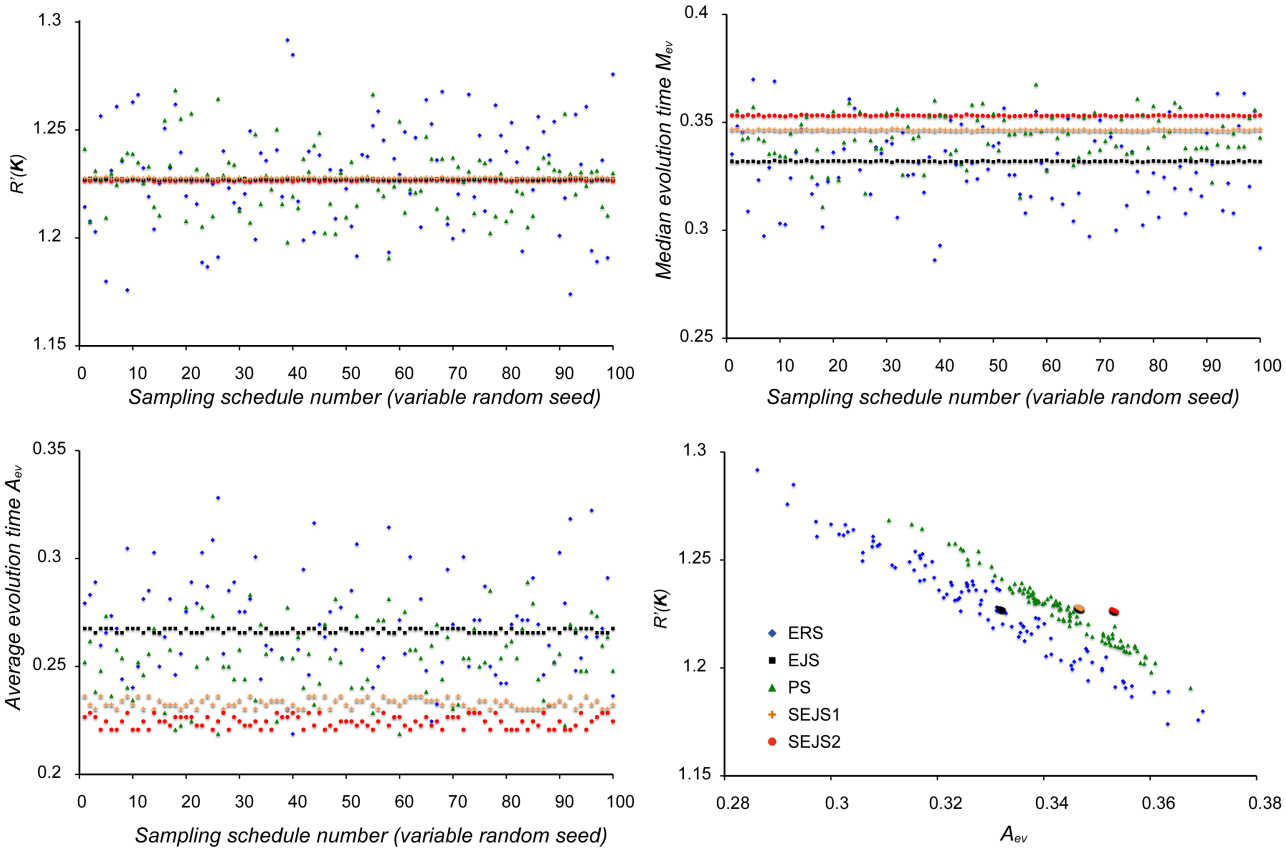

*Figure 3 Sensitivity (R'(**K**)) and resolution parameters (A_{ev} and M_{ev}) plotted for the first 100 schedules (of 1000) generated for the five different approaches to NUS discussed (ERS, EJS, PS, SEJS1 and SEJS2).*

For each of the 1000 sampling schedules generated for each NUS approach the PSF of the corresponding sampling function was calculated. The $\bar{M}_{PSF}$, σ_{PSF} and *PSR* parameters were calculated for each PSF and the average and standard deviation of these values are given in Table 2 and summarised in Fig. 4. In contrast to the sampling schedule dependent parameters it can be seen that the variation of the various parameters about the mean is similar in all cases. The skewed distributions of the sine-weighted sampling approaches correlate with reduced noise content as measured by $\bar{M}_{PSF}$ and σ_{PSF} as well as increased sensitivity as measured by PSR. There was also a noticeable trend between the $\bar{M}_{PSF}$ and the $\sigma_{PSF,}$, especially clear for the jittered sampling approaches. This suggests that a reduction of the average sampling noise is associated with a larger spread of the noise amplitudes about the mean, which is likely a manifestation of Parceval's theorem. Furthermore, there is a correlation between the relative sensitivity of the sampling schedule as measured by *R'(**K**)* and the sampling nosie level as measured by the $\bar{M}_{PSF}$ for all non-jittered approaches. This is consistent with gains in sensitivity in the PSF beign related to denser sampling of earlier time points.

Table 2 *The average and standard deviation of PSF related parameters. 1000 sampling schedules were generated using different random seeds for five different NUS approaches (same as Table 1). The PSF of these schedules was calculated and used to derive statistics of sensitivity related parameters. ERS: random samples from an exponentially decaying probability distribution. EJS: jittered random samples from an exponentially decaying probability distribution. PS: Poisson gap sampling with shifted sine weighting. SEJS1: jittered random samples from an exponentially decaying probability distribution augmented with a shifted sine weighting. SEJS2: same as SEJS1 but with different decay and sine weighting.*

	ERS	EJS	PS	SEJS1	SEJS2
PSR	5.32	5.09	5.38	5.38	5.61
St. dev.	0.54	0.52	0.54	0.54	0.54
$\bar{M}_{PSF}$	0.51	0.52	0.51	0.51	0.50
St. dev.	0.01	0.01	0.01	0.01	0.01
σ_{PSF}	0.28	0.29	0.28	0.28	0.27
St. dev.	0.01	0.01	0.01	0.01	0.01

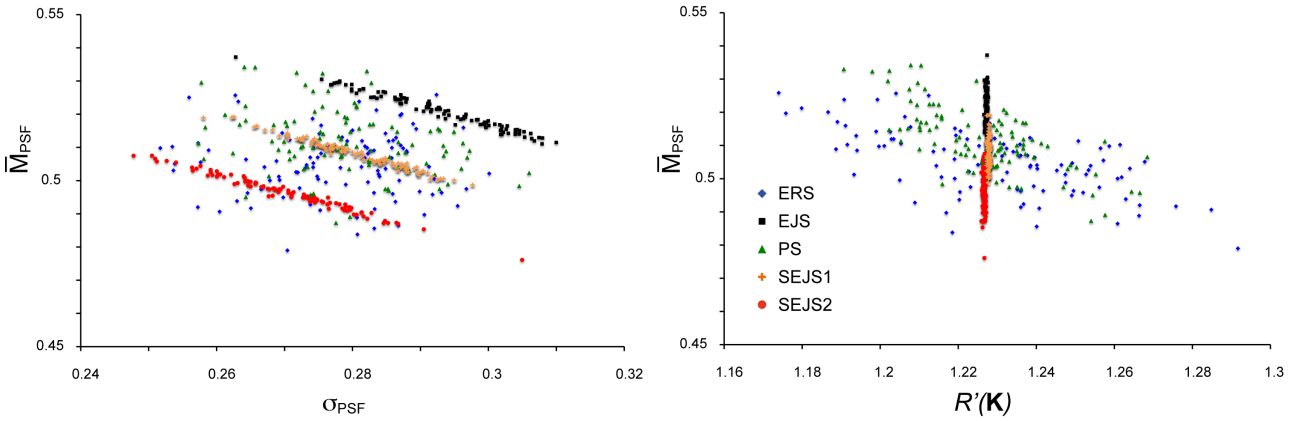

Figure 4 *Plot on left shows the correlation between the average and standard deviation of the sampling related noise (from the PSF). The plot on the right shows the correlation between the average of the sampling related noise and the sensitivity of the corresponding sampling schedule as measured by R'(**K**). The plots are based on the first 100 schedules (of 1000) generated for the five different NUS approaches to NUS described (ERS, EJS, PS, SEJS1 and SEJS2).*

The PSF with the best (highest) and worst (lowest) PSR for each method was identified and is shown in Fig. 5. As discussed above the PSR was taken as the ratio between the 0 Hz frequency component and the highest artifact outside the peak region. A total of 20 points (~200 Hz) either side of the 0 Hz frequency component were excluded such that data points making up the linewidth introduced by the exponential weighting of the sampling schedules would not be included as artifacts. It can be seen that for the ERS scheme this has led to the selection of a schedule that has strong artifacts in this region (note this is about a third of the shaded region in Fig. 5). For the jittered and Poisson methods the PSFs of the schedules that generate the worst PSRs have strong spikes at the extremes of the spectral window, these artifacts are due to the pseudorandom nature of the sampling by these method. In extreme cases these pseudorandom methods impose order on the sampling schedule, which on the one hand shifts the artifacts to extreme frequencies, and on the other hand concentrates these at frequencies where aliasing artifacts would be expected. There is a known relationship between oversampling, NUS and aliasing, which has been discussed in detail previously [17, 27, 28]. It should be noted that the amplitude of the strongest artifacts in all cases is comparable regardless of the method used.

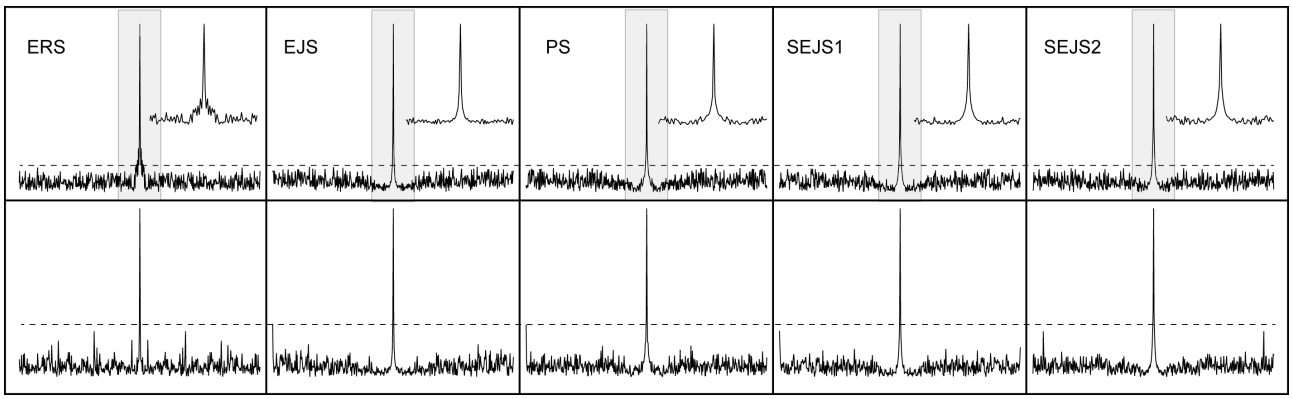

Figure 5 *The figure shows PSFs generated from the different sampling schemes tested here. The top panels show the PSFs of the schedules that generated the highest (best) PSRs and the bottom panels show the schedules that generated the lowest (worst) PSRs. The NUS approach used is given at the top left of each column. The inset shows an expansion of the shaded area. Note that although the sampling noise level and the magnitude of the largest artifacts are comparable in all cases, the pseudo-random nature of Poisson-gap and jittered sampling methods result in the largest artifacts being shifted to the extremes of the spectral window, whilst conversely the region near the central component contains the smallest artifacts. The dashed line marks the highest amplitude artifacts across each row of PSFs.*

2D schedules

The jittered sampling algorithm discussed above is easily extendable to multiple dimensions. The multidimensional implementation is exemplified here by generation of a number of 2D sampling schedules with different probability distributions (see Fig. 6). The figure shows exactly 512 jitter regions each having a different colour according to a heat map going from black to purple, red and finally yellow. The heat map colouring is also consistent with the probability density, going from high to low probability according to the above order. The black region will contain the point in the PDF that has the highest probability weighting (in the case where there is no weighting the order is based on the evolution time going from low to high, along each dimension).

Each heat map plot has the same number of jitter regions of the same colour. All regions are approximately equiprobably, containing ~1/512 of the total probability density. The size of each jitter region is therefore dependent on the probability of the points it encompasses, such that regions containing parts of the PDF with a high probability weighting will be smaller and areas of the PDF that have a low probability weighting will be larger. Note that exactly one sample is taken from each region, such that areas containing large jittered regions will be sampled less densely than areas containing many small regions.

To demonstrate how the sampling regions are modified depending on the underlying PDF, a synthetic Nyquist grid was defined with 64 x128 points in dimensions 1 and 2 with spectral widths of 2000 and 16000 Hz in each dimensions. These parameters were chosen to mimic a standard triple resonance experiment with or without constant time acquisition in the two indirect dimensions (e.g. HNCACB at 900 MHz). In each case 512 points were subsampled from the 8192 available points (6.25%). Four scenarios were tested each having a different PDF; *i*) with no weighting in either dimension *ii*) exponential weighting in only dimension 2, corresponding to a linewidth of 50 Hz *iii*) exponential weighting in both dimensions, corresponding to linewidths of 20 and 50 Hz in dimensions 1 and 2 and finally *iv*) sine weighting as defined by Eq. 6, using α and β parameters of 0.6 and 8, in both dimensions (see also section *Approximation of sine weighted Poisson-gap sampling* for implementation of sine weighting in 2D). The sine weight parameters were the same as those used in the 1D case (SEJS1) to mimic the weighting of the Poisson gap sampling method.

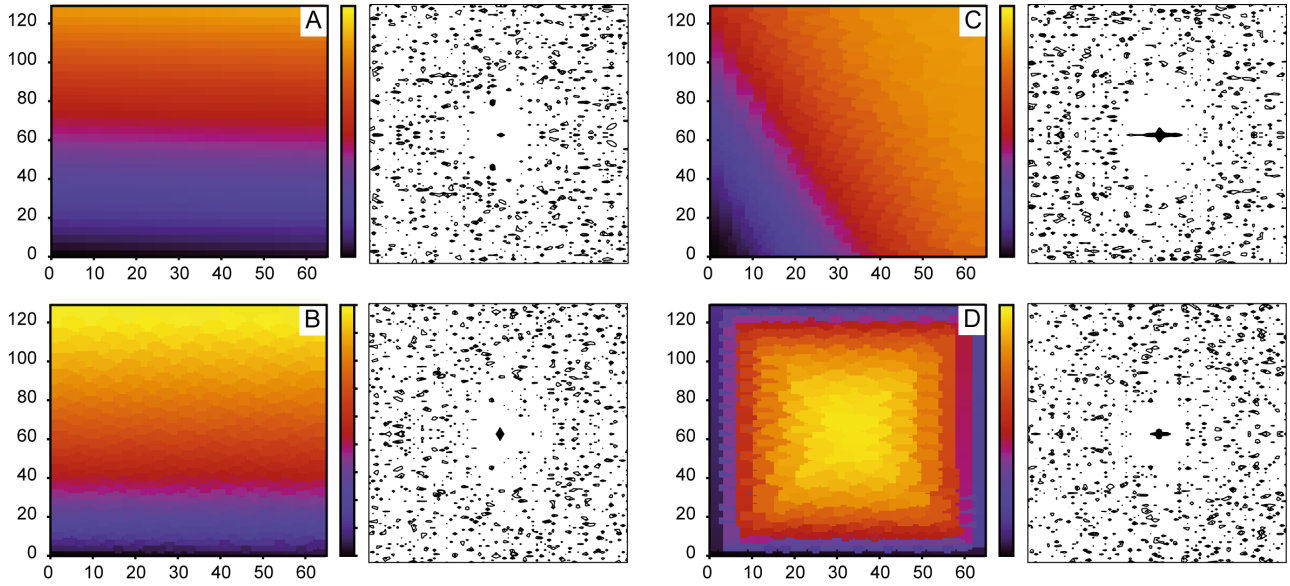

Figure 6 *The figures shows the distribution and size of different jittered sampling regions (color coded heat map) based on different probability density functions (PDF). The incremented coordinates of the time domain are marked on the axes of the heat map. Each jitter region is represented by a different colour and the probability of each region is approximately the same. As the weighting is increased the darker regions (black/purple) become smaller, whilst the lighter regions (yellow, red) become larger. Exactly one point is sampled from each region, such that an area containing many small regions (see near origin of C) is sampled more densely than an area containing fewer larger regions (see centre of D). The jittered regions are used to generate a sampling schedule for which the corresponding PSF is also shown (black and white). The underlying Nyquist grid is constructed loosely based on the ^{15}N (64 points) and ^{13}C (128 points) dimensions of triple resonance experiments typically used for protein backbone assignments (e.g. HNCACB at 900 MHz). 512 points were selected from the 8192 point grid. A) Example where jittered sampling is used without any weighting of the PDF (constant time in both dimensions). B) Jittered sampling used without exponential weighting in one dimension (constant time ^{15}N). C) Jittered sampling using exponential weighting in both dimensions (constant time in neither dimension). D) Jittered sampling with sine weighting in both indirect dimensions of the PDF (similar to SEJS above).*

*R'(**K**)* was computed for 1000 schedules with the parameters described above, using either jittered sampling or random sampling. As for the 1D case (see Figs 3 and 4), the jittered sampling schedules showed much less seed dependence than those generated by random sampling. The range of values for jittered sampling ranged from 1.437 to 1.448 (standard deviation 0.002), whereas the extremes of random sampling were 1.302 and 1.517 (standard deviation of 0.032).

Experimental data

Finally, the jittered sampling algorithm was compared to ERS when applied to an experimental 3D HNCO dataset, having constant time (no decay) along the ^{15}N dimension and an exponential decay along the ^{13}C dimension. The linewidth of the ^{13}C dimension was measured using linear sampling without apodisation and found to be ~16 Hz, this was subsequently used to calculate *R'(**K**)* for all sampling schedules generated. Linewidth parameters that produce the same average *R'(**K**)* were

used to generate 1000 ERS and EJS sampling schedules having decay rates roughly twice the natural linewidth in ^{13}C (30 for EJS and 28 for ERS). A total of 75 points were sampled from a grid of 52 ^{15}N and 128 ^{13}C increments (total N = 6656), equating to *ca* 1% of the total sampling space. For ERS and EJS the sampling schedule with the highest and lowest ***R'(K)*** were selected and a plane at a proton frequency of 8.14 ppm was reconstructed using maximum entropy (same plane as used in previous examples [10, 14]). The same maximum entropy reconstruction parameters were used for all reconstructions shown in Fig. 7 (*def* = 0.01, *aim* = 0.05). The ratio between the weakest signal and the highest artifact was measured together with the linewidth of one of the peaks, to monitor for relative changes in sensitivity and resolution. As expected the ERS method showed a larger spread of ***R'(K)*** values compared to EJS, which resulted in noticeable variability in sensitivity and resolution.

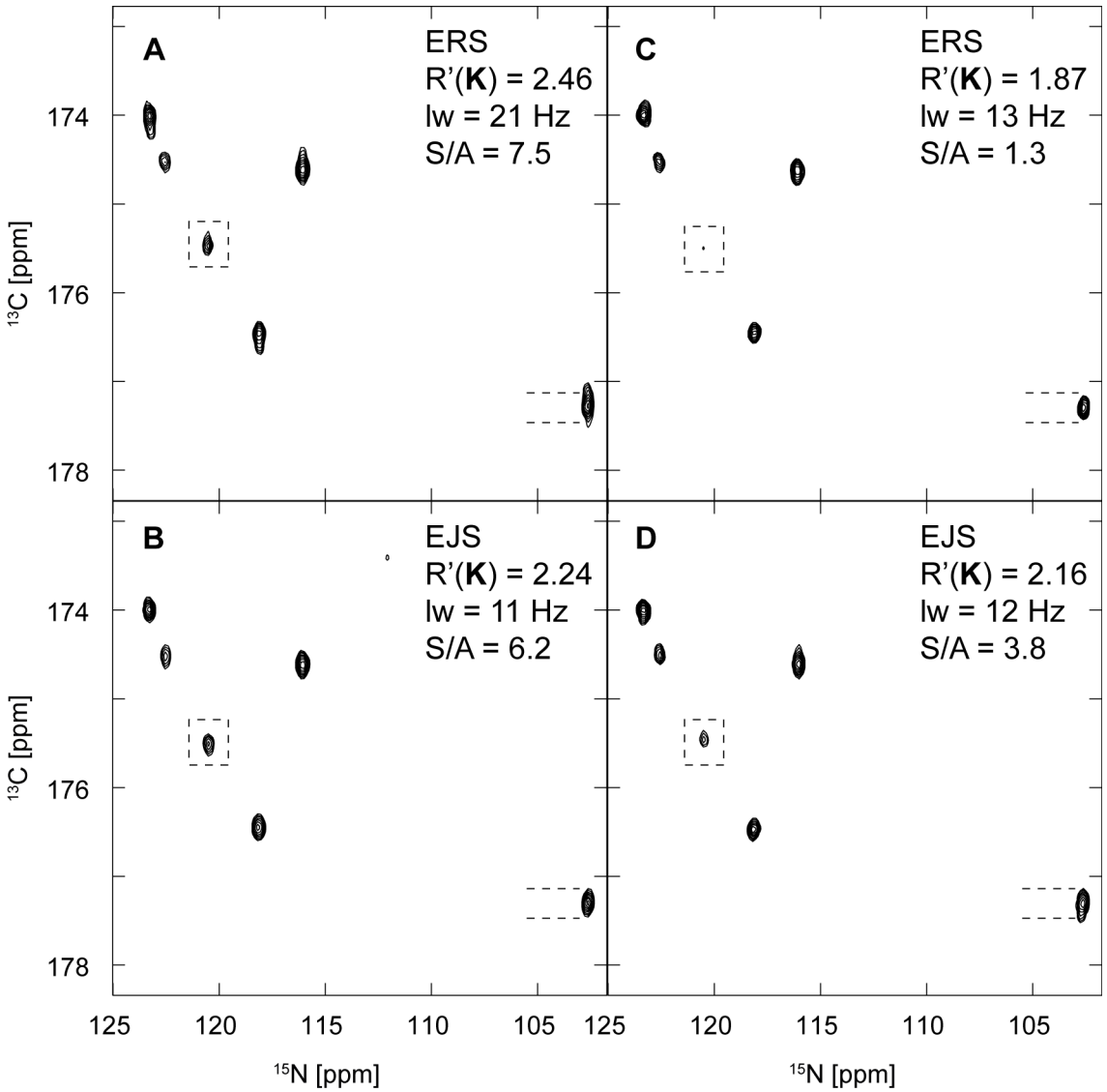

*Figure 7 Panel A and C show spectral representation of an HNCO plane using the schedule with the highest and lowest R'(**K**) using exponentially weighted random sampling (ERS) at twice the natural decay of the signals. Panels B and D show the same when using exponentially weighted random jittered sampling (EJS). The contour level is set at the same level in all spectra and chosen to show the weakest peak (dotted box). The two dashed lines are separated by the same distance in each panel and the measured linewidth of the peak is reported as lw in each panel. In each case the ratio between the weakest peak and the most intense artifact is reported (S/A).*

Discussion

Non-uniform sampling using jittered sampling (JS) appropriate for on-grid sampling and arbitrary probability density functions (PDFs) was introduced for multidimensional NMR spectroscopy. The algorithm produces sampling schedules with relative sensitivities $R'(\boldsymbol{K})$ showing very little random seed dependence. The performance of jittered sampling was compared to the commonly applied approaches to NUS, namely random sampling (RS) and Poisson-gap sampling (PS). It was found that the random seed dependence of both RS and PS, as measured by a range of sampling schedule related parameters, show much higher variability than JS (See Fig. 4). In general, the spectral properties of PS, as measured by a range of metrics associated with the PSF, could be replicated by JS when the appropriate sampling distribution was used. In 1D NUS, both JS and PS were found to produce PSFs that have characteristic blue shifted noise as described previously [20], where sampling related artifacts are shifted to higher frequencies, minimizing artifacts in the immediate vicinity of the 0 Hz signal (see also Fig. 5). It was also found for both JS and PS that the most intense artifacts, as identified by the PSR parameter, were shifted close to the edges of the spectral window, consistent with these methods being more likely than random sampling methods to produce schedules with more intense aliasing artifacts. The intensity of these artifacts was, however, not significantly larger than the most intense artifacts found for random sampling (See Fig. 5). In general the PSR parameter was most sensitive to the underlying PDF, increasing for distributions that were skewed to the right, i.e. having a larger average evolution time and a smaller median evolution time. The trend of increased PSR when skewing the distribution to the right may account for some of the positive outcomes seen for PS in the past such as lower average sampling noise [21]. It is also noted that the PSFs using the recently described multidimensional Poisson-gap sampling method do not produce schedules with PSFs that have the characteristic "blue noise" (data not shown), consistent with previous reports [10]. As noted above the weaving approach used to extend the method to multiple dimensions does not restrict the distance between points that are in different rows/columns/planes. Although the samples may have a Poisson distribution in each row/column/plane, they will not necessarily adhere to this distribution as a multidimensional object. This departure from the Poisson distribution is likely the cause of the absence of the blue shifted noise.

As expected, a correlation between the average evolution time and the inherent sensitivity of the sampling function as defined by $R'(\boldsymbol{K})$ was found. There is, however, also an interesting trend, found only for RS and PS, between the relative sensitivity of the sampling schedule as measured by $R'(\boldsymbol{K})$ and the average of sampling noise ($\overline{M}_{PSF}$), see Fig. 4. This trend is not present for JS due to the very low variation of $R'(\boldsymbol{K})$ when using this method. It should therefore be noted that if the noise contents of the PSF, as measured by $\overline{M}_{PSF}$, is minimised to find an "optimal" sampling schedule for a set of PS/RS parameters [26], it is most likely that this will instead skew the outcome to a schedule that has unusually low average evolution time. Although this may produce sampling schedules with higher sensitivity, the same can be achieved more effectively by increasing the exponential weighting in the PDF. The latter would also reduce the average evolution time, but in a more direct manner. As noted above, JS shows little seed dependent variation in relative sensitivity, as measured by $R'(\boldsymbol{K})$, thus if the above procedure of minimising $\overline{M}_{PSF}$ to find an optimal schedule is followed the results will not be biased by variation in $R'(\boldsymbol{K})$.

In the 2D case we find that the implementation of JS showed much the same trends as in 1D, again showing significant reduction in seed dependent variation in relative sensitivity, $R'(\boldsymbol{K})$, compared to RS. The consequence of these trends are demonstrated by the experimental data in Fig. 7 where it is clear that for RS, extremes of $R'(\boldsymbol{K})$ produce highly variable results. Where a schedule is chosen with the lowest $R'(\boldsymbol{K})$ the weakest peak in the spectrum is barely detectable above the lowest artifact (7C), whereas noticeable line broadening is found where the schedule with the highest $R'(\boldsymbol{K})$ is chosen (7A). No such variability was found for JS (Fig. 7 B and D).

Currently, there are no standardised procedures for reporting NUS data. Often there is simply a statement that the data was acquired using NUS, with a reference to the reconstruction method used. In some cases the decay parameters as well as the algorithm used to generate the NUS schedule is reported. The random seed used to generate the data is never reported (to the best

knowledge of the author) and even if it was, the random number generators are commonly platform specific and therefore do not guarantee that the same random subset is select on different systems. The sampling schedule itself is not required to be stored in central databases, and is not commonly included in the published work. The work presented here shows that for commonly applied NUS methods the information that is reported is insufficient for accurately replicating the work, a central requirement of scientific reports. The strength of the jittered sampling approach, therefore, lies in producing random sampling schedules that result in highly reproducible data.

The described algorithm is here implemented for spectrometer use for up to 4D data. The JS approach is computationally more demanding than the RS code previously described, due to the requirement of generating the appropriate jittering regions. However, for the typical case of 3D experiments (2 indirect dimensions), the program produces a JS schedule in a few seconds. In the 4D case (3 indirect dimensions) the JS schedules are typically generated in less than a minute. But, for very large 4D datasets with many regions, this procedure can take several minutes to complete on a spectrometer PC and may be best done "off-line".

Conclusions

Here an algorithm is described for on-grid jittered sampling appropriate for any probability density function and dimensionality. Spectra generated from NUS data, based on the same probability density function and the same maximum evolution time were shown to have a significant variation in their relative sensitivity. The relative sensitivity of NUS schemes is known to significantly impact on the line shape and sensitivity of the reconstructed spectra. Here, it was shown that by dividing the regions of the PDF into equiprobable regions and selecting a sample from each of those regions, it is possible to generate random sampling schedules that have similar relative sensitivities whilst having the desirable properties of a random distribution. It was found that the relative sensitivity of a sampling schedule is correlated with several parameters used for evaluating or optimising the associated point spread function. Since different jittered sampling schedules generated based on the same PDF do not show significant variation in their relative sensitivity, it is expected that the described method will enable more reproducible data to be generated when using NUS, as well as, providing a means of NUS optimisation without sensitivity bias.

Acknowledgments

The author is indebted to many fruitful discussions with Prof. Jeffrey Hoch, Drs Alan Stern, Mark Maciejewski, Viktor Vegh and Adam Schuyler. The HNCO dataset was originally acquired by Dr Mark Maciejewski at the University of Connecticut. I wish to thank Dr Wolfgang Bermel (Bruker Biospin) for help in developing the spectrometer interface for the sampling schedule generator. MM is supported by an ARC Future Fellowship (FTl10100925).

References

[1] M. Ikura, L.E. Kay, A. Bax, A novel approach for sequential assignment of proton, carbon-13, and nitrogen-15 spectra of larger proteins: heteronuclear triple-resonance three-dimensional NMR spectroscopy. Application to calmodulin, Biochemistry, 29 (1990) 4659-4667.
[2] M. Mobli, J.C. Hoch, Nonuniform sampling and non-Fourier signal processing methods in multidimensional NMR, Progress in Nuclear Magnetic Resonance Spectroscopy, 83 (2014) 21-41.
[3] S. Sibisi, J. Skilling, R.G. Brereton, E.D. Laue, J. Staunton, Maximum entropy signal processing in practical NMR spectroscopy, Nature, 311 (1984) 446-447.
[4] J.C.J. Barna, S.M. Tan, E.D. Laue, Use of CLEAN in conjunction with selective data sampling for 2D NMR experiments, Journal of Magnetic Resonance, 78 (1988) 327-332.

[5] V.Y. Orekhov, I.V. Ibraghimov, M. Billeter, MUNIN: A new approach to multi-dimensional NMR spectra interpretation, J. Biomol. NMR, 20 (2001) 49-60.
[6] K. Kazimierczuk, W. Kozminski, I. Zhukov, Two-dimensional Fourier transform of arbitrarily sampled NMR data sets, J Magn Reson, 179 (2006) 323-328.
[7] A.S. Stern, D.L. Donoho, J.C. Hoch, NMR data processing using iterative thresholding and minimum l1-norm reconstruction, Journal of Magnetic Resonance, 188 (2007) 295-300.
[8] D.J. Holland, M.J. Bostock, L.F. Gladden, D. Nietlispach, Fast Multidimensional NMR Spectroscopy Using Compressed Sensing, Angewandte Chemie International Edition, 50 (2011) 6548-6551.
[9] K. Kazimierczuk, V.Y. Orekhov, Accelerated NMR Spectroscopy by Using Compressed Sensing, Angewandte Chemie International Edition, 50 (2011) 5556-5559.
[10] J.C. Hoch, M.W. Maciejewski, M. Mobli, A.D. Schuyler, A.S. Stern, Nonuniform Sampling and Maximum Entropy Reconstruction in Multidimensional NMR, Accounts of Chemical Research, 47 (2014) 708-717.
[11] S.G. Hyberts, H. Arthanari, S.A. Robson, G. Wagner, Perspectives in magnetic resonance: NMR in the post-FFT era, Journal of Magnetic Resonance, 241 (2014) 60-73.
[12] S. Paramasivam, C.L. Suiter, G. Hou, S. Sun, M. Palmer, J.C. Hoch, D. Rovnyak, T. Polenova, Enhanced sensitivity by nonuniform sampling enables multidimensional MAS NMR spectroscopy of protein assemblies, J Phys Chem B., 116 (2012) 7416-7427.
[13] D. Rovnyak, J.C. Hoch, A.S. Stern, G. Wagner, Resolution and sensitivity of high field nuclear magnetic resonance spectroscopy, J Biomol NMR, 30 (2004) 1-10.
[14] M. Mobli, A.S. Stern, J.C. Hoch, Spectral reconstruction methods in fast NMR: Reduced dimensionality, random sampling and maximum entropy, Journal of Magnetic Resonance, 182 (2006) 96-105.
[15] J.C. Hoch, M.W. Maciejewski, B. Filipovic, Randomization improves sparse sampling in multidimensional NMR, Journal of Magnetic Resonance, 193 (2008) 317-320.
[16] J.C.J. Barna, E.D. Laue, M.R. Mayger, J. Skilling, S.J.P. Worrall, Exponential sampling, an alternative method for sampling in two-dimensional NMR experiments, Journal of Magnetic Resonance (1969), 73 (1987) 69-77.
[17] M. Mobli, J.C. Hoch, Maximum entropy spectral reconstruction of nonuniformly sampled data, Concept Magnetic Res, 32 (2008) 436-448.
[18] M. Palmer, B. Wenrich, P. Stahlfeld, D. Rovnyak, Performance tuning non-uniform sampling for sensitivity enhancement of signal-limited biological NMR, Journal of Biomolecular NMR, 58 (2014) 303-314.
[19] M. Lustig, D. Donoho, J.M. Pauly, Sparse MRI: The application of compressed sensing for rapid MR imaging, Magnetic Resonance in Medicine, 58 (2007) 1182-1195.
[20] K. Kazimierczuk, A. Zawadzka, W. Koźmiński, Optimization of random time domain sampling in multidimensional NMR, Journal of Magnetic Resonance, 192 (2008) 123-130.
[21] S.G. Hyberts, K. Takeuchi, G. Wagner, Poisson-gap sampling and forward maximum entropy reconstruction for enhancing the resolution and sensitivity of protein NMR data, J Am Chem Soc, 132 (2010) 2145-2147.
[22] M. Bostock, D. Holland, D. Nietlispach, Compressed sensing reconstruction of undersampled 3D NOESY spectra: application to large membrane proteins, Journal of Biomolecular NMR, 54 (2012) 15-32.
[23] S. Hyberts, H. Arthanari, G. Wagner, Applications of Non-Uniform Sampling and Processing, in: M. Billeter, V. Orekhov (Eds.) Novel Sampling Approaches in Higher Dimensional NMR, Springer Berlin Heidelberg, 2012, pp. 125-148.
[24] M. Mobli, A.S. Stern, W. Bermel, G.F. King, J.C. Hoch, A non-uniformly sampled 4D HCC(CO)NH-TOCSY experiment processed using maximum entropy for rapid protein sidechain assignment, Journal of Magnetic Resonance, 204 (2010) 160-164.
[25] D. Rovnyak, M. Sarcone, Z. Jiang, Sensitivity enhancement for maximally resolved two-dimensional NMR by nonuniform sampling, Magnetic Resonance in Chemistry, 49 (2011) 483-491.

[26] P.C. Aoto, R.B. Fenwick, G.J.A. Kroon, P.E. Wright, Accurate scoring of non-uniform sampling schemes for quantitative NMR, Journal of Magnetic Resonance, 246 (2014) 31-35.
[27] G.L. Bretthorst, Nonuniform Sampling: Bandwidth and Aliasing, in: J. Rychert, G. Erickson, C.R. Smith (Eds.) Maximum Entropy and Bayesian Methods in Science and Engineering, Springer, New York, 2001, pp. 1-28.
[28] M.W. Maciejewski, H.Z. Qui, I. Rujan, M. Mobli, J.C. Hoch, Nonuniform sampling and spectral aliasing, J Magn Reson, (2009).